

Computation of the Streamfunction and Velocity Potential for Limited and Irregular Domains

ZHIJIN LI* AND YI CHAO

Jet Propulsion Laboratory, California Institute of Technology, Pasadena, California

JAMES C. MCWILLIAMS

Department of Atmospheric Science, and Institute of Geophysics and Planetary Physics, University of California, Los Angeles, Los Angeles, California

(Manuscript received 22 November 2004, in final form 14 December 2005)

ABSTRACT

An algorithm is proposed for the computation of streamfunction and velocity potential from given horizontal velocity vectors based on solving a minimization problem. To guarantee the uniqueness of the solution and computational reliability of the algorithm, a Tikhonov regularization is applied. The solution implies that the obtained streamfunction and velocity potential have minimal magnitude, while the given velocity vectors can be accurately reconstructed from the computed streamfunction and velocity potential. Because the formulation of the minimization problem allows for circumventing the explicit specification of separate boundary conditions on the streamfunction and velocity potential, the algorithm is easily applicable to irregular domains. By using an advanced minimization algorithm with the use of adjoint techniques, the method is computationally efficient and suitable for problems with large dimensions. An example is presented for coastal oceans to illustrate the practical application of the algorithm.

1. Introduction

Streamfunction and velocity potential are used extensively in meteorology and oceanography. In low latitudes, geostrophic balance breaks down as the Coriolis parameter becomes small, and streamfunction and velocity potential are more suitable scalar variables for depicting flow patterns than other variables, such as pressure and geopotential heights, that are more suitable for large-scale flow patterns in middle latitudes (e.g., Palmer 1952). Streamfunction and velocity potential are also more suitable for analyzing flow patterns when spatial scales are smaller than the Rossby radius of deformation. Recently, streamfunction and velocity

potential have attracted much attention for their use in data assimilation. In a data assimilation algorithm, it is necessary to model error self-correlations of velocity components and cross correlations between velocity components (e.g., Cohn 1997; Lorenc 1986). The anisotropy and inhomogeneity of the self-correlations and large values of the cross correlations make them difficult to represent appropriately in a data assimilation algorithm (Daley 1991, chapter 5; Lorenc et al. 2000). In both the analysis of flow patterns and the estimation of error correlations in data assimilation, it is thus frequently desirable to compute streamfunction and velocity potential from velocity vectors.

The computation of streamfunction and velocity potential from velocity vectors can easily be carried out over the global domain. However, for a limited domain, the computation is complicated by boundaries, and the methods currently used are based on various assumptions for handling boundary conditions (Sangster 1960; Shukla and Saha 1974; Bijlsma et al. 1986; Lynch 1988; also see section 2). More physically sound and computationally efficient methods are desirable for limited domains.

* Additional affiliation: Raytheon Technical Services Co. LLC, Pasadena, California.

Corresponding author address: Dr. Zhijin Li, Jet Propulsion Laboratory, California Institute of Technology, M/S 300-323, 4800 Oak Grove Dr., Pasadena, CA 91109.
E-mail: zhijin.li@jpl.nasa.gov

Most methods for the computation of streamfunction and velocity potential have been applied to regular domains, while there is an increasing need for complex domains. Recently, the number of velocity measurements from radars has been rapidly increasing. While Doppler radar can provide nearly time-continuous three-dimensional (3D) velocity measurements in the atmosphere (National Research Council 2002), high-frequency (HF) radar can measure the sea surface water velocity (Puduan and Graber 1997). The radar-measured velocity is generally available only in limited irregular domains. In addition, an irregular domain is unavoidable in a variety of other circumstances. For example, in coastal oceans, irregular coastline shapes and island distributions are ubiquitous. Similarly, when streamfunction and velocity potential are computed using the height coordinate in the atmosphere, the computational domain becomes irregular in the presence of mountains. As far as we know, there are not yet standard methods for computing streamfunction and velocity potential for such complex domains.

In this paper, we propose a new algorithm for computing streamfunction and velocity potential from horizontal velocity vectors. This algorithm can easily be implemented on irregular domains. Also, the algorithm is computationally efficient and, thus, can be used for problems with large dimensions.

The outline of this paper is as follows. Section 2 reviews the theoretical and computational issues. In section 3, the new algorithm is formulated. Computational examples are presented in section 4. Finally, section 5 summarizes the features of the new algorithm.

2. The decomposition problem

According to the Helmholtz theorem, the horizontal velocity vector \mathbf{v} can be decomposed into nondivergent and irrotational components,

$$\mathbf{v} = \mathbf{v}_\psi + \mathbf{v}_\chi, \quad (1)$$

where

$$\mathbf{v}_\psi = \mathbf{k} \times \nabla\psi, \quad \mathbf{v}_\chi = \nabla\chi, \quad (2)$$

ψ is the streamfunction, χ the velocity potential, and ∇ the horizontal gradient vector. Taking the vertical component of the curl of (1), we get

$$\nabla^2\psi = \zeta, \quad (3)$$

where ζ is the vertical component of the relative vorticity. Similarly, taking the divergence of (2), we have

$$\nabla^2\chi = D, \quad (4)$$

where D is the horizontal velocity divergence.

For the global domain, the periodic boundary condition allows the decomposition problem (1) to have a unique solution and makes it straightforward to solve. For a limited domain, however, the solution of the partitioning problem (1) is not unique, because equal and opposite flows with zero vorticity and divergence can be added to ψ and χ without affecting the total velocity (Gent and McWilliams 1983; Lynch 1989). For a given velocity field in a limited domain, there could be an infinite number of partitioning solutions. Additional conditions are necessary for a unique partitioning solution.

There are two approaches in the literature for specifying the partitioning uniquely for limited domains. While Lynch (1989) proposes a three-component partitioning, most existing methods apply boundary conditions to Poisson's equations given by (3) and (4) to obtain uniquely defined ψ and χ . Here, we are concerned with the latter one. There are two types of boundary conditions for Poisson equations: the Dirichlet type and the Neumann type. The Dirichlet type requires specifying the values of ψ and χ at the boundaries. The Neumann type requires specifying the normal derivatives of ψ and χ at the boundary.

Various approximated boundary conditions have been suggested, and the Poisson equations are then solved for obtaining a determined solution for ψ and χ . For example, Sangster (1960) proposed the boundary condition of the Dirichlet type: first, let $\chi = 0$ at the boundary to solve (4) for χ , and second the boundary value of ψ is specified by integrating $-\partial\psi/\partial s = \mathbf{v}_n - \partial\chi/\partial n$. Lynch (1989) discussed as many as eight methods for specifying the boundary condition, which can be the Dirichlet or Neumann type, as well as their combination. Some physically sound methods are also used for specifying the boundary conditions. One such method is to minimize the divergent kinetic energy, which leads to the boundary condition $\partial\psi/\partial n = \mathbf{n} \cdot \mathbf{v}$ (e.g., Lynch 1989). One drawback of the above-mentioned methods is that the velocity reconstructed from the computed ψ and χ may not well match the original velocity field. In practice, these methods need to be refined. One method to refine them is to use an iterative procedure to adjust the solution, and this iterative method can help in some cases as shown in Shukla and Saha (1974) and Bijlsma et al. (1986). Though the iterative method is a widely used method, it still has both numerical and computational limitations. First, there is no guarantee that the iteration will converge (Lynch 1988). Second, it is computationally costly, since each iteration requires a solution for the Poisson equations, and a large number (say 60) of iterations are usually needed to obtain a satisfactory result (Shukla and Saha 1974).

While the above-described methods for approximately specifying boundary conditions have been applied to regular domains, it is more difficult to apply them to irregular domains, especially to problems like coastal oceans where islands are present. Watterson (2001) recently proposed a method for computing streamfunction and velocity potential for oceans. In this method, it is assumed that ψ is a constant along a continuing coastline, which implies that the flow is nondivergent along the coastline. As demonstrated by Watterson (2001), this may be an acceptable approximation for basin scales in some cases. Unfortunately, the nondivergence assumption becomes invalid for those coastal regions where there exists pronounced Ekman transport in association with upwelling/downwelling, such as the U.S. and African west coasts. To specify ψ and χ at such boundaries is practically impossible. For irregular domains with the presence of islands, the specified boundary conditions can even be in conflict and lead to the nonexistence of a solution. For example, the approximation for specifying ψ by integrating $\partial\psi/\partial s = v_n$ can no longer be used. To circumvent such difficulties, we herein propose a method that does not require explicitly specifying boundary conditions, while a unique decomposition is obtained.

3. Algorithm based on a Tikhonov regularization

The computation of velocity vectors from the streamfunction and velocity potential and the computation of the streamfunction and velocity potential from velocity vectors typically compose a pair of direct and inverse problems (e.g., Kirsch 1996). The former is the direct and well-posed problem, while the latter is the inverse and ill-posed problem.

The above-described inverse problem actually is a classic one in inverse problem theory (Tikhonov and Arsenin 1977). It is known that Tikhonov's regularization is a reliable method to solve this type of inverse problem. We propose here an algorithm based on Tikhonov's regularization.

To derive our proposed algorithm, we consider the discrete form of (2). A traditional, centered, second-order finite-difference approximation is adopted for simplicity. This is equivalent to the well-known Arakawa "C" grid (Arakawa and Lamb 1977). The arrangement of variables is shown in Fig. 1. Since the streamfunction is defined on the central grid points, the discretization as in Fig. 1 is not the same as that typically used, in which the streamfunction is defined on the corner grid points as given in Lynch (1988). The discretization in Fig. 1 offers some convenience in incorporating physical boundary conditions, such as those

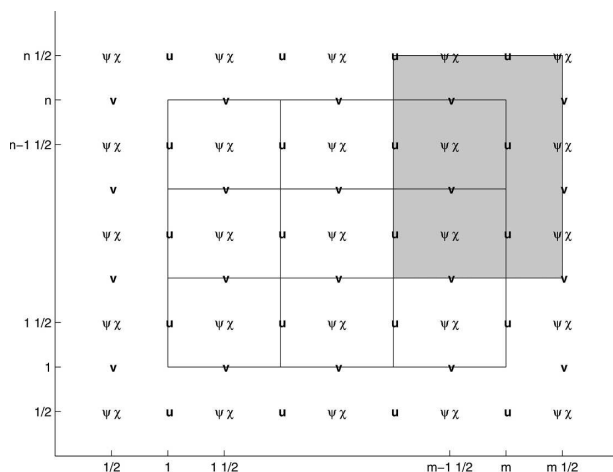


FIG. 1. Illustration of the Arakawa C grid. The shadowed area represents a land area for coastal ocean problems.

due to coastlines, and the physical boundary condition of zero normal velocity at the coastlines can be easily incorporated.

We arrange u at the grid points into a vector \mathbf{u} , then \mathbf{u} is a $m(n+1)$ vector. In the same way, we arrange v at the grid points into a vector \mathbf{v} , then \mathbf{v} is a $n(m+1)$ vector. Similarly, we have a $(m+1)(n+1)$ vector $\boldsymbol{\psi}$ arranging ψ at the grid points, and a $(m+1)(n+1)$ vector $\boldsymbol{\chi}$ arranging χ at the grid points. By these definitions, the discrete form of (1) becomes a linear system of the form

$$\mathbf{y} = \mathbf{A}\mathbf{x}, \quad (5)$$

where

$$\mathbf{x} = \begin{pmatrix} \boldsymbol{\psi} \\ \boldsymbol{\chi} \end{pmatrix}, \quad \mathbf{y} = \begin{pmatrix} \mathbf{u} \\ \mathbf{v} \end{pmatrix}, \quad (6)$$

\mathbf{x} is an N vector [$N = 2(m+1)(n+1)$], \mathbf{y} an M vector [$M = m(n+1) + (m+1)n$], and \mathbf{A} is an M by N matrix. The matrix \mathbf{A} depends on the discretization scheme.

The same form of equation as in (5) can still be used for irregular domains, such as coastal oceans where coastline and islands are present. As an example, consider a single land area present in the domain as shown by the shaded area in Fig. 1. In this case, given the particular arrangement of the variables on the grid points, we just need to mask out all the variables over this land area; that is, all the variables on land are set to zero, and then we do not need to change the dimensions of \mathbf{x} , \mathbf{y} , and \mathbf{A} .

Equation (5) can be used to reconstruct the velocity vector \mathbf{y} , but cannot be used directly to solve for \mathbf{x} inversely. This is because \mathbf{A} is not a square matrix due to the fact of $M < N$, and the inverse problem is un-

deretermined. We may specify appropriate boundary conditions to reduce the degrees of the freedom of \mathbf{x} (Lynch 1988, 1989). However, such appropriate boundary conditions are difficult to prescribe as discussed in section 2. Particularly, it is practically impossible to specify appropriate boundary conditions for domains, such as coastal oceans with the presence of separate land areas.

Since it is practically impossible to invert (5) directly, we have to seek an alternative method to solve this inverse problem. One possible method is to seek a generalized solution. To seek a generalized solution, a commonly used method is to determine the best fit in the sense that one tries to minimize the objective functional $\|\mathbf{Ax} - \mathbf{y}\|$ with respect to \mathbf{x} in terms of a defined norm. When the Eulerian norm is used, the objective functional has the quadratic form

$$J(\mathbf{x}) = \frac{1}{2} (\mathbf{y} - \mathbf{Ax})^T (\mathbf{y} - \mathbf{Ax}), \quad (7)$$

where the superscript T stands for transpose. In addition, $J(\mathbf{x})$ is half the error variance of the velocity that is reconstructed from the computed ψ and χ . When $J(\mathbf{x})$ is zero, the velocity vector can be perfectly reconstructed from the computed ψ and χ .

The minimum of (7) can be found analytically for some cases. One case is when the boundary conditions are given, the dimension of \mathbf{x} is not larger than that of \mathbf{y} , plus the rank of \mathbf{A} is equal to the dimension of \mathbf{x} . In this case, $\mathbf{A}^T \mathbf{A}$ is invertible. Let the derivative of $J(\mathbf{x})$ be zero; that is, $\nabla_{\mathbf{x}} J(\mathbf{x}) = 0$. We immediately obtain the solution that minimizes $J(\mathbf{x})$:

$$\mathbf{x} = (\mathbf{A}^T \mathbf{A})^{-1} \mathbf{A}^T \mathbf{y}, \quad (8)$$

where \mathbf{A}^T is the transpose of \mathbf{A} , also known as the adjoint of \mathbf{A} . The solution (8) is then the Moore–Penrose pseudoinverse or the left pseudoinverse, often denoted by \mathbf{A}^+ . When \mathbf{A} is invertible, the solution is the same as the one obtained by directly inverting (5). Another case is for when the rank of \mathbf{A} is equal to the dimension of \mathbf{y} ; we then have the solution

$$\mathbf{x} = \mathbf{A}^T (\mathbf{A} \mathbf{A}^T)^{-1} \mathbf{y}, \quad (9)$$

which is often referred to as the right pseudoinverse or data-space inverse in geophysical applications. In this case, the boundary condition may not necessarily be specified explicitly.

However, we do not use (8) or (9) to solve our problems when \mathbf{x} has a large dimension. To compute the pseudoinverse of \mathbf{A} requires a singular vector decomposition of \mathbf{A} . For a problem with a very large dimension, the pseudoinverse of \mathbf{A} can be computed with

particular methods, such as those from the Arnoldi Package software (ARPACK; e.g., Lehoucq et al. 1998), but the computational load is not acceptable when a large number of singular vectors of \mathbf{A} are necessary. One may note that the singular vectors need only be computed a single time, and then just used repeatedly. This can reduce the computational cost, but it requires significant computer memory to store the singular vectors and thus is subject to the availability of computer memory. In addition, the input of huge datasets is not a good choice for parallel computers, since the input and output can be a bottleneck in parallel computing. Further, for a problem with large dimensions, only a portion of the singular vectors of \mathbf{A} may be allowed to be computed. When only a limited number of singular vectors are used, the accuracy of the reconstructed velocity can be a concern.

We thus need to seek other alternative methods that are suitable for problems with large dimensions, and have no requirement of the explicit specification of boundary conditions while guaranteeing the accuracy of the reconstructed velocity.

We propose to use the Tikhonov regularization method (Tikhonov and Arsenin 1977), which is a classic method for solving an ill-posed inverse problem. With a Tikhonov regularization, a regularization term is introduced to the objective functional (7), and it has the form

$$\begin{aligned} J_{\alpha}(\mathbf{x}) &= \frac{1}{2} (\mathbf{y} - \mathbf{Ax})^T (\mathbf{y} - \mathbf{Ax}) + \alpha \frac{1}{2} \mathbf{x}^T \mathbf{x} \\ &= J(\mathbf{x}) + J_{\text{reg}}(\mathbf{x}), \end{aligned} \quad (10)$$

where the parameter α is a positive parameter, called the regularization parameter, and $J_{\alpha}(\mathbf{x})$ is called Tikhonov's functional. The minimizer of $J_{\alpha}(\mathbf{x})$ can then be interpreted as that obtained when the streamfunction and velocity potential tend to be the minimal magnitude, while the reconstructed velocity field tends to be the "best" fit to the original velocity. The regularization term J_{reg} has a particular physical meaning; that is, minimizing J_{reg} is equivalent to minimizing the opposing irrotational, nondivergent components of \mathbf{v}_{ψ} and \mathbf{v}_{χ} (Gent and McWilliams 1983; Lynch 1989). In fact, these components are always excluded at the minimum of $J_{\alpha}(\mathbf{x})$ as we will prove later. Due to the regularization term, $J_{\alpha}(\mathbf{x})$ has a unique minimum \mathbf{x}_{α} (see theorem 2.11 in Kirsch 1996).

After the regularization term is applied, the minimum of the objective functional depends on the regularization parameter α . In fact, α causes an approximation in the sense that the minimum of $J_{\alpha}(\mathbf{x})$ is not necessarily the minimum of $J(\mathbf{x})$. We can illustrate this

approximation by considering the case where \mathbf{u} and \mathbf{v} can be perfectly reconstructed. In this case, $J(\mathbf{x})$ is zero, but $J(\mathbf{x})$ may not be zero at the minimum of $J_\alpha(\mathbf{x})$. Certainly, we do not expect to perfectly reconstruct \mathbf{u} and \mathbf{v} , but it is necessary that $J(\mathbf{x})$ has an acceptably small value at the minimum \mathbf{x}_α . Ideally, we should use the optimal α , at which point $J(\mathbf{x})$ reaches the smallest value. To find such an optimal α , a complicated a posteriori choice can be used, and such an optimal α can always be found (Kirsch 1996, chapter 2). For our problem, however, it turns out that α has a broad range of values that produce acceptably small values of $J(\mathbf{x})$, and thus a simple trial and error procedure can serve well in finding an appropriate α . We will discuss further the determination of α by this trial and error procedure in section 4, where the computational example is given.

The Tikhonov functional given in (10) can be reliably and efficiently minimized with advanced minimization algorithms and adjoint techniques. During the last two decades, several minimization algorithms have been developed for solving problems with large dimensions. The most frequently used algorithms include quasi-Newton limited memory type algorithms and preconditioned conjugate gradient algorithms (e.g., Nocedal and Wright 1999).

When these two types of minimization algorithms are applied to complicated problems, the adjoint technique is necessary. Both types require the gradient of the Tikhonov functional. By differentiating the Tikhonov functional, we obtain the gradient

$$\nabla_{\mathbf{x}} J_\alpha(\mathbf{x}) = -\mathbf{A}^T(\mathbf{y} - \mathbf{Ax}) + \alpha\mathbf{x}. \quad (11)$$

Equation (11) shows that the gradient can be computed by applying \mathbf{A}^T to $(\mathbf{y} - \mathbf{Ax})$, and it is noteworthy that this operation incurs the same computational cost as the computation of \mathbf{Ax} .

Using the adjoint technique to compute the gradient deserves more explanation. With a higher-order differencing scheme and complex coastline and isolated islands, it is almost impossible to express \mathbf{A} explicitly. What we know about \mathbf{A} often comes only through a computer program, such as a Fortran program, for computing velocity from the streamfunction and velocity potential. The adjoint \mathbf{A}^T can be developed directly from the computer program (e.g., Navon et al. 1992). As such, the adjoint technique offers multiple benefits. First, the computed gradient is accurate to the computer precision; second, the adjoint technique can be applied to very sophisticated models; third, it is applicable to problems with large dimensions, since \mathbf{A} and its adjoint matrix \mathbf{A}^T do not need to be stored, but only the vector $\mathbf{A}^T(\mathbf{y} - \mathbf{Ax})$ needs to be retained; and fourth, the computation can be efficient.

After having examined in detail the computational aspects of the Tikhonov regularization-based algorithm, we shall here discuss the properties of the solution obtained with the algorithm.

We have pointed out the problem of nonuniqueness. The nonuniqueness implies that there exist nonzero vectors \mathbf{e} , which satisfy

$$\mathbf{A}\mathbf{e} = 0. \quad (12)$$

That is, \mathbf{A} has a nontrivial null space. To make the solution unique is essentially to make a choice to get a determined \mathbf{e} in the null space. We examine next this determined \mathbf{e} in the solution.

Let the null space of \mathbf{A} be spanned by $\mathbf{e}_1, \mathbf{e}_2, \dots, \mathbf{e}_K$, where $K > 0$ is the dimension of the null space. The minimizer of (10) can always be decomposed as

$$\mathbf{x}_\alpha = \mathbf{x}_\beta + \sum_{k=1}^K c_k \mathbf{e}_k, \quad (13)$$

where c_k are constant coefficients and \mathbf{x}_β has no projection in the null space; that is,

$$\mathbf{e}_k^T \mathbf{x}_\beta = 0. \quad (14)$$

By replacing \mathbf{x}_α into (11), we can then obtain $c_k = 0$ at the minimum, which satisfies $\nabla_{\mathbf{x}} J_\alpha(\mathbf{x}_\alpha) = 0$ (see the appendix). Thus, the component on the null space is excluded in the solution due to the Tikhonov regularization.

As discussed before, we know that the component on the null space of \mathbf{A} can arise from two aspects: first, equal and opposite flows with zero vorticity and divergence can be added to ψ and χ without affecting the total velocity (Gent and McWilliams 1983); and second, necessary boundary conditions are not specified. Since those equal and opposite flows are not physically meaningful, it is reasonable to minimize them as in Lynch (1989), and it is desirable to exclude them as in our solution. The justification for the exclusion of the component on the null space due to the unspecified boundary conditions is a practical issue. It can be practically justified if the obtained ψ and χ can approximately satisfy (5) and (6), and this is true when $J(\mathbf{x})$ is approximately zero at the minimum.

Another relevant question is whether the solution is related to the solution of (3) and (4) with the Dirichlet and Neumann boundary conditions. Again, when $J(\mathbf{x})$ is approximately zero at the minimum, the solution approximately satisfies (5) and (6). Because of the uniqueness of the decomposition, the normal derivatives of the streamfunction and velocity potential in (5) and (6) are thus approximately but uniquely determined at the boundaries. The solution with the deter-

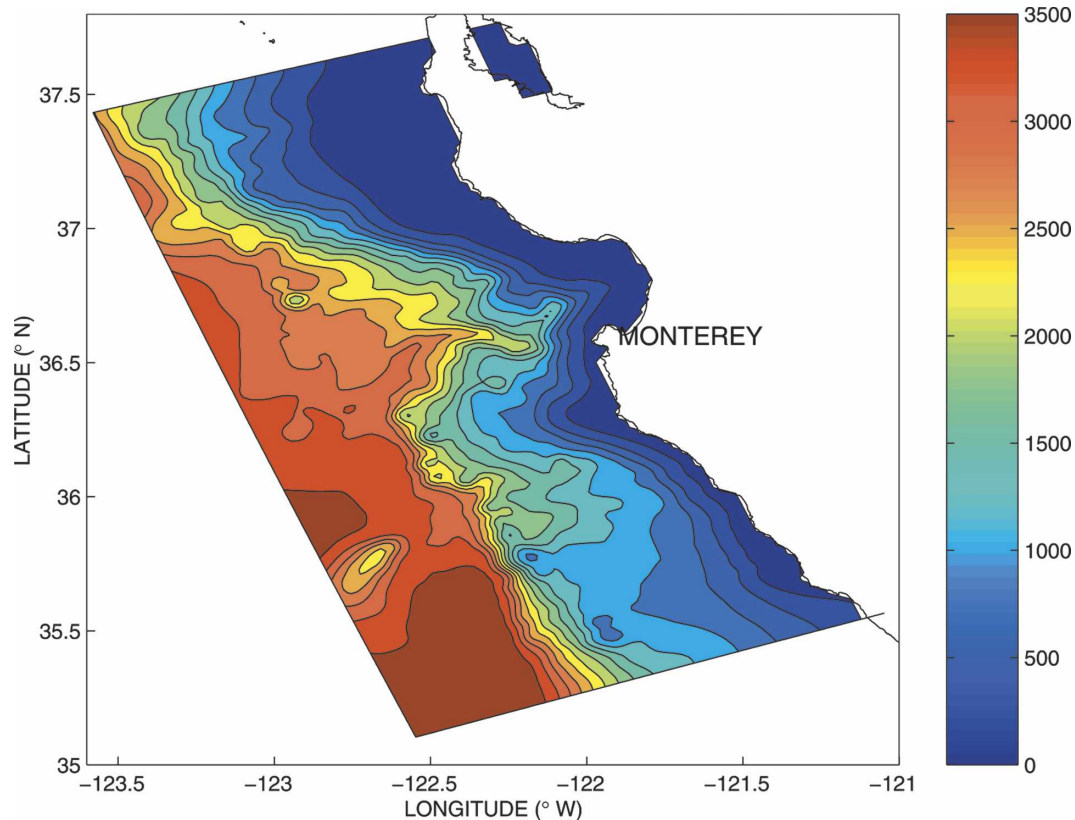


FIG. 2. The model domain and bathymetry (m). The contour interval is 250 m.

mined normal derivatives is thus related to the solution of (3) and (4) with the Neumann condition at the boundaries.

4. A computational example

The dataset used for demonstrating the proposed algorithm is derived from a three-dimensional Regional Ocean Modeling System (ROMS) (Shchepetkin and McWilliams 1998, 2003; Marchesiello et al. 2001, 2003). In this study, ROMS is implemented in a three-level nested configuration. The first level covers the U.S. west coast (USWC) ocean at 15-km resolution, the second level covers the central California coastal (CCC) ocean at 5-km resolution, and the third level fits the Monterey Bay (MB) at 1.5-km resolution. All the of three nesting levels have 20 vertical sigma layers. A one-way nesting scheme is implemented (Blayo and Debreu 1999). In this study, only the 1.5-km ROMS output is used for the computation of streamfunction and velocity potential.

The model domain is bounded by the coastline on the eastern side, and the bathymetry shows a bay and canyon (Fig. 2). A curvilinear horizontal coordinate is

used, and thus the grid distribution is irregular to some degree. There are 186 grid points alongshore, and 88 grid points cross shore. The streamfunction and velocity potential are analyzed at the physical height levels. A masking technique is used to differentiate the land and sea grid points.

The ROMS output used is from a data assimilation exercise using August 2003 conditions when the Autonomous Ocean Sampling Network (AOSN) Monterey Field Experiment was implemented in the area surrounding Monterey Bay, California (Chao et al. 2006, manuscript submitted to *Deep-Sea Res.*). The surface forcing is derived from the output of the Coupled Ocean/Atmospheric Model Prediction System (COAMPS) (Hodur 1997) with a horizontal resolution of 3 km.

To demonstrate the proposed method, we choose a transition from an upwelling event to a relaxation period, during which the velocity field underwent rapid and complex changes. Figure 3 presents the sea surface current and temperature at a depth of 10 m. The temperature is shown here to illustrate the transition from an upwelling event to a relaxation period. During the upwelling period on 16 and 18 August, the nearshore

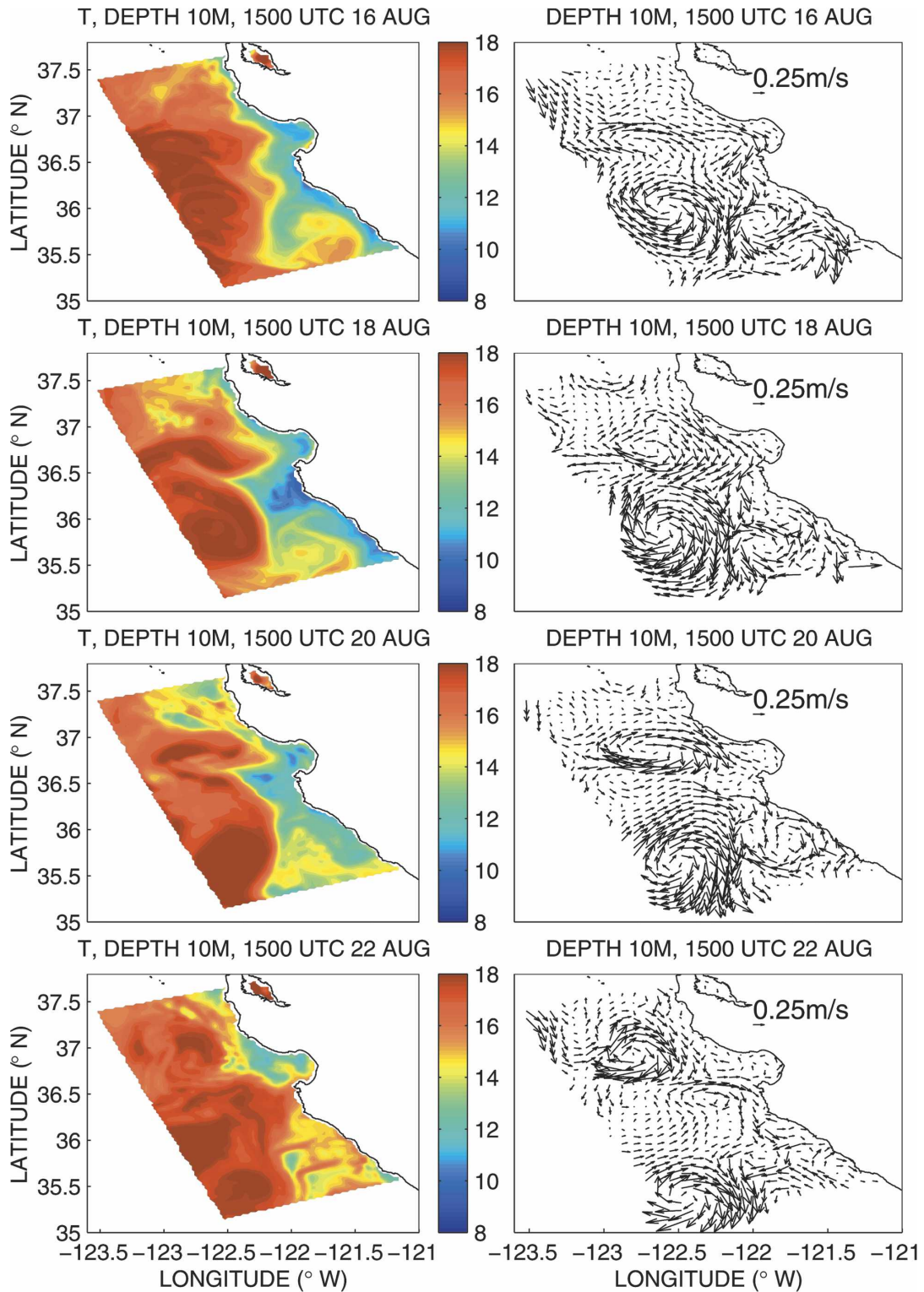


FIG. 3. The evolution of temperature and velocity vectors at a depth of 10 m. Both 16 and 18 Aug are during the upwelling event, while 20 and 22 Aug are during the relaxation.

temperature is as cold as 10° – 12° C. In association with the upwelling, there is an equatorward current jet with a width of about 50 km along the coastline. During the relaxation period on 20 and 22 August, the temperature becomes warmer near shore. Another prominent difference during the relaxation is that the equatorward current jet is weakened substantially. Interestingly, a few small-scale eddies form after the equatorward current jet is weakened. In the area to the east of the jet, there was a major anticyclonic eddy, which moved from 36° N on 18 August to 35.5° N on 22 August.

Figure 4 presents the streamfunctions and velocity potentials derived from the velocity vectors in Fig. 3. During the upwelling, the streamfunctions show a band with lower values and a width of about 25 km along the coastline. The lower values of the streamfunction are consistent with the lower temperatures there. During the relaxation, a well-defined small-scale eddy forms between 36° and 35.5° N, and is well represented in the streamfunction.

As is well known, Ekman transport drives upwelling. During upwelling, Ekman transport drives near-surface water off shore, and thus horizontal divergence dominates near surface along the coastline. Consistent with this dynamical scenario, the divergence is dominant along the coastline during upwelling on 16 and 18 August; that is, the velocity potential is lower along the coastline. In contrast, during the relaxation on 20 and 22 August, the velocity potential is dominated by higher centers, which correspond to convergence centers.

The velocity potential interestingly displays fine structures along the coastline. We expect to find convergence upstream of a headland. Such a convergence center can be found at 37° N, and also at the tip of the Monterey Peninsula on 16 and 18 August, when the equatorward upwelling jet prevails. Thus, the computed velocity potential can represent fine convergence structures related to the curvature of the coastline.

In summary, the computed streamfunction reasonably represents the upwelling pattern and the eddies from meso- to small scale. The velocity potential reasonably describes the divergence and convergence during the upwelling and relaxation time. The small-scale divergence and convergence centers related to the curvature of the coastline are also well represented.

In section 2, we stated that the assumption of the constant streamfunction along a coastline becomes invalid for upwelling regions because of strong convergence and divergence. In Fig. 4, the streamfunction displays significant variations along the coastline. The large gradient of the streamfunction along the coastline corresponds to the centers of velocity potential, which

in turn correspond to the divergence and convergence centers. The statement is supported by the computation.

Now let us examine the accuracy of the velocity vectors reconstructed from the streamfunctions and velocity potentials. Figure 5 shows the difference between the original velocity and the reconstructed velocity. The differences are smaller than 0.005 m s^{-1} . The overall accuracy should be quite acceptable since the error is less than 1% of the typical velocity. The spatial distribution of the error is also satisfactory, since the error is largest in the relatively intense current areas. The error is especially small near the boundaries, which suggests that the boundary condition is well controlled.

We have pointed out that the accuracy depends on the regularization parameter. The smaller the Tikhonov regularization parameter, the more accurate the reconstructed velocity is. A larger Tikhonov regularization parameter reduces the accuracy by making the reconstructed velocity field smoother. In practice, the velocity field tends to be noisy, and it may not be desirable to reconstruct the velocity field at a high accuracy. The choice of the value of the regularization parameter can be used as a trade-off between accuracy and smoothness.

To determine a particular value of the regularization parameter, we can follow a rule of thumb to make a first guess, and then use a trial and error procedure to refine it. The first guess of α can be estimated with the formula of $|\mathbf{v}|^2/100|\psi|^2$, where $|\mathbf{v}|$ is the averaged velocity over the domain and $|\psi|$ is the averaged streamfunction over the domain. Such an α generally results in errors in the reconstructed velocity of less than a few percents. In our computation here, the regularization parameter is 10^{-11} . This number is obtained since $|\mathbf{v}|$ is about 0.3 m s^{-1} and $|\psi|$ is about 10^4 s^{-1} . We have tested the method with values of this parameter ranging from 10^{-10} to 10^{-12} , and the results are qualitatively the same, and the error is reduced by about 1.5% as the parameter decreases from 10^{-10} to 10^{-12} . These results suggest that a reasonable accuracy in the reconstructed velocity vector can be achieved over a broad range of regularization parameters.

5. Summary and discussion

A new method has been proposed to compute streamfunction and velocity potential from velocity vectors. This method is applicable to irregular domains. Thus, it can be applied to coastal ocean problems with complex coastlines and isolated islands, and limited area atmospheric problems even in nonterrain-following vertical coordinates, in which the horizontal level may intersect mountains.

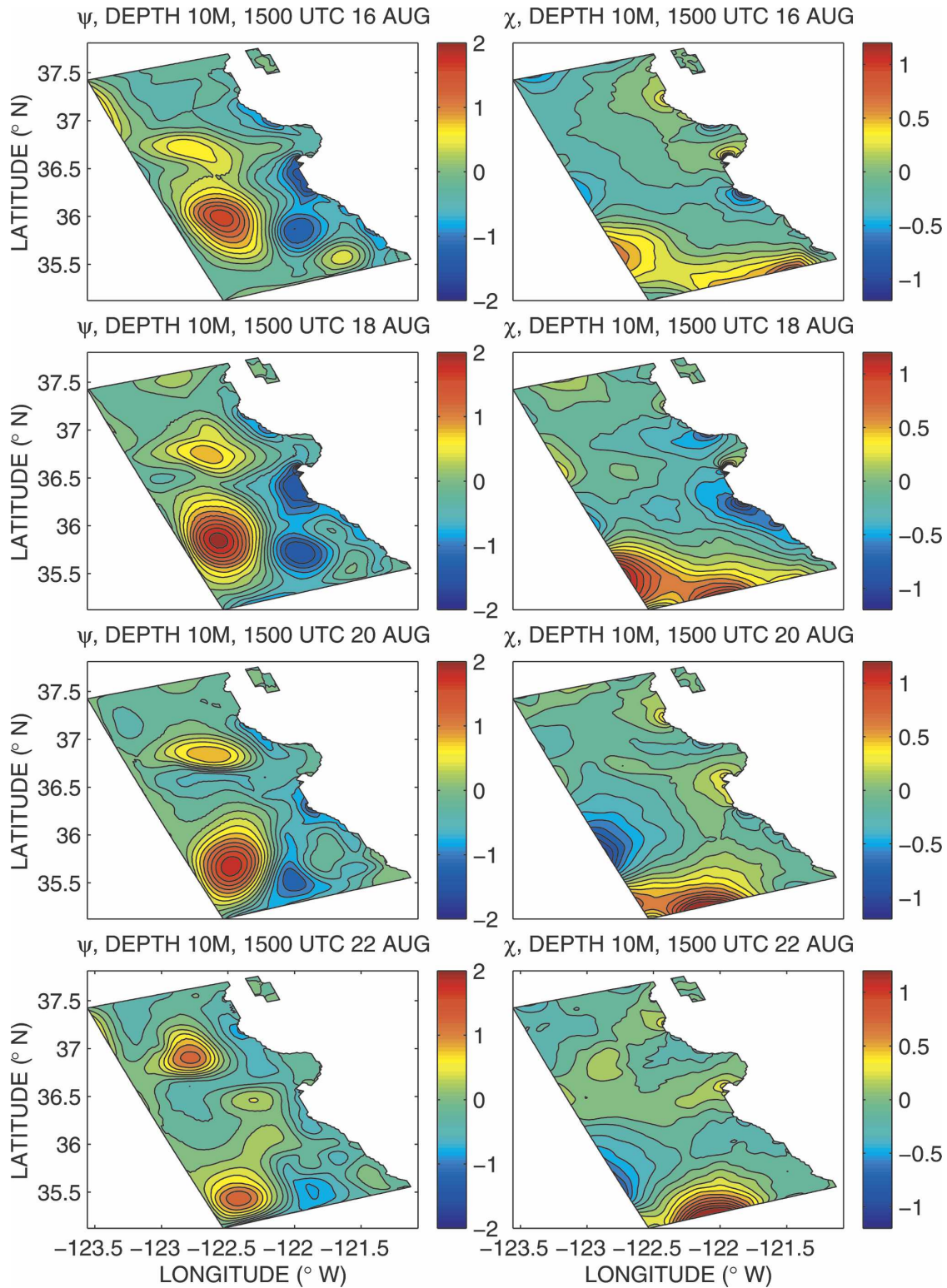


FIG. 4. The computed streamfunction ψ and velocity potential χ corresponding to the velocity vectors in Fig. 3 (10^4 s^{-1}).

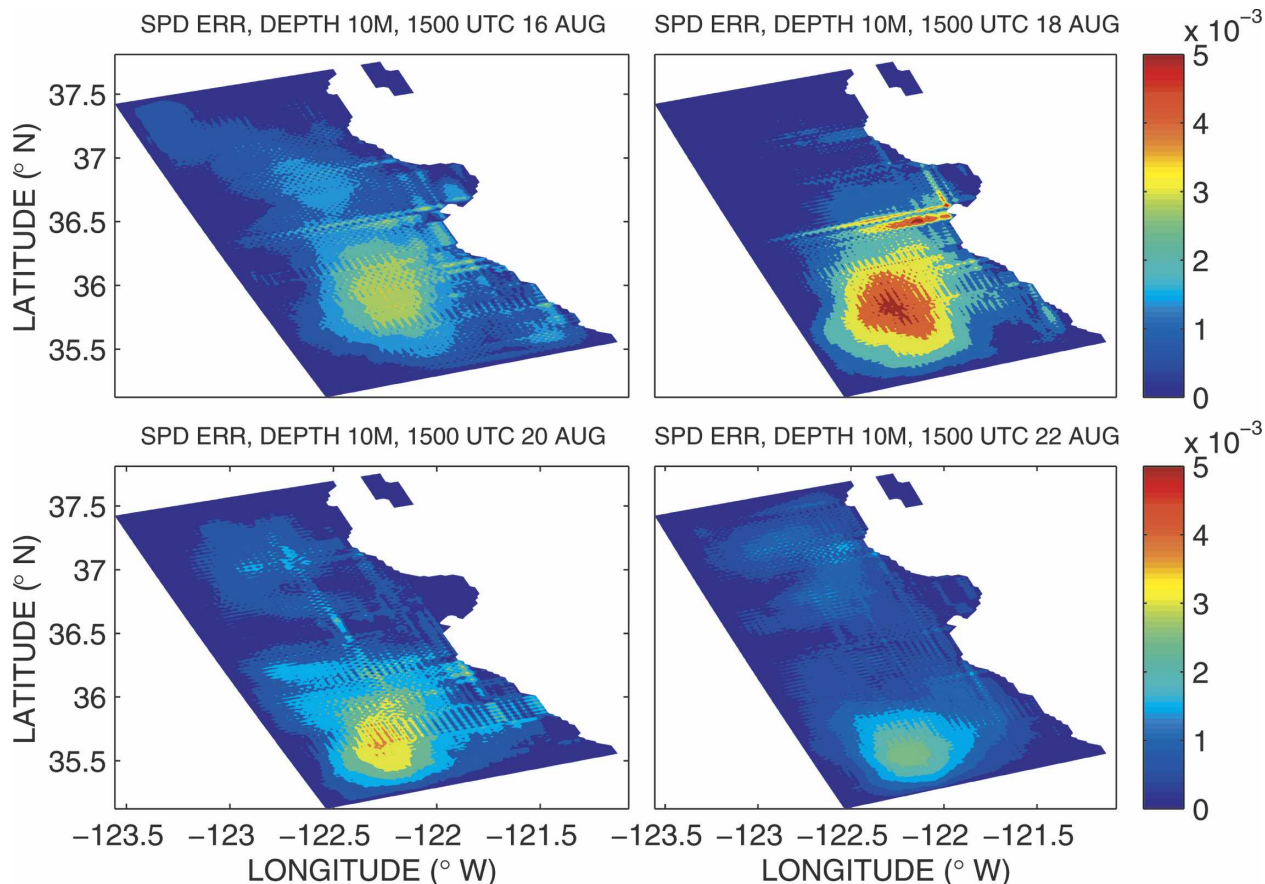


FIG. 5. The difference between the reconstructed velocity vectors in Fig. 4 and the original velocity vectors in Fig. 3 (m s^{-1}).

Following inverse problem theory, the computation of the streamfunction and velocity potential is transformed into a minimization problem. The classic Tikhonov regularization is introduced to guarantee the uniqueness of the solution. In this minimization problem, explicit specification of the conditions at computational boundaries conditions is circumvented, and the minimization problem implicitly determines these boundary conditions. For physical boundary conditions, such as those due to coastline, the specification can be circumvented, but it can also still be specified. Since the boundary conditions for irregular domains are difficult to specify, the circumvention of the specification of the boundary condition renders the algorithm especially easy to apply to such domains. Another benefit that the algorithm offers is that we do not need to know the explicit form of the matrix \mathbf{A} in (5), by which we compute velocity vectors from streamfunction and velocity potential, but we only need the matrix-vector product $\mathbf{A}\mathbf{x}$, that is, a method for computing \mathbf{u} and \mathbf{v} from ψ and χ .

The regularized minimization methodology not only

renders the algorithm applicable to irregular domains, but also has powerful computational potential for large-scale problems. The computational efficiency is obtained by applying advanced minimization algorithms and the adjoint technique. In this study, we use the quasi-Newton limited memory method (Liu and Nocedal 1989). Using the example described in section 4 as a guide we estimate that a problem with on the order of 10^5 grid points can be solved in a few minutes on today's commonly available workstations. The computational efficiency and the technique of the implicit computation of \mathbf{A} allows the method to be applied to problems with dimensions larger than this example.

Acknowledgments. The research described in this publication was carried out, in part, at the Jet Propulsion Laboratory (JPL), California Institute of Technology, under a contract with the National Aeronautics and Space Administration (NASA). Computations were performed on the SGI Origin computer through the JPL Supercomputing Project. We are grateful to Dr. James Doyle at the Navy Research Laboratory

for preparing the atmospheric forcing from the Coupled Ocean/Atmospheric Model Prediction System (COAMPS). We thank Drs. Patrick Marchesiello and Xavier Capet at the University of California, Los Angeles, for their help with the ROMS setup. Thanks also go to Dr. Jichun Li at the University of Nevada, Las Vegas, and Dr. Kayo Ide at the University of California, Los Angeles, for stimulating discussions. The authors thank Dr. John Farrara for his careful review of the manuscript. Dr. Watterson and one anonymous reviewer are acknowledged for their insightful comments. Support from the Office of Naval Research (ONR) through the Autonomous Ocean Sampling Network (AOSN) project is also acknowledged.

APPENDIX

The Proof of $\mathbf{c}_k = \mathbf{0}$

The minimum \mathbf{x}_α satisfies $\nabla_{\mathbf{x}} J_\alpha(\mathbf{x}_\alpha) = \mathbf{0}$; that is,

$$-\mathbf{A}^T(\mathbf{y} - \mathbf{A}\mathbf{x}_\alpha) + \alpha\mathbf{x}_\alpha = \mathbf{0}. \quad (\text{A1})$$

Since $\mathbf{A}\mathbf{e}_k = \mathbf{0}$, the substitution of (13) into (A1) gives

$$-\mathbf{A}^T(\mathbf{y} - \mathbf{A}\mathbf{x}_\beta) + \alpha\left(\mathbf{x}_\beta + \sum_{k=1}^K c_k \mathbf{e}_k\right) = \mathbf{0}. \quad (\text{A2})$$

The inner product of \mathbf{e}_k with (A2) yields

$$-(\mathbf{A}\mathbf{e}_k)^T(\mathbf{y} - \mathbf{A}\mathbf{x}_\beta) + \alpha\mathbf{e}_k^T\mathbf{x}_\beta + \alpha c_k = 0. \quad (\text{A3})$$

Since $\mathbf{A}\mathbf{e}_k = \mathbf{0}$ and $\mathbf{e}_k^T\mathbf{x}_\beta = 0$, we obtain $c_k = 0$.

REFERENCES

- Arakawa, A., and V. R. Lamb, 1977: Computational design of the basic dynamical processes of the UCLA general circulation model. *Methods in Computational Physics*, J. Chang, Ed., Vol. 17, Academic Press, 173–265.
- Bijlsma, S. J., L. M. Hafkenscheid, and P. Lynch, 1986: Computation of the streamfunction and velocity potential and reconstruction of the wind fields. *Mon. Wea. Rev.*, **114**, 1547–1551.
- Blayo, E., and L. Debreu, 1999: Adaptive mesh refinement for finite-difference ocean models: First experiments. *J. Phys. Oceanogr.*, **29**, 1239–1250.
- Cohn, S. E., 1997: Estimation theory for data assimilation problems: Basic conceptual framework and some open questions. *J. Meteor. Soc. Japan*, **75**, 257–288.
- Daley, R., 1991: *Atmospheric Data Assimilation*. Cambridge Atmospheric and Space Science Series, Cambridge University Press, 457 pp.
- Gent, P. R., and J. C. McWilliams, 1983: Consistent balanced models in bounded and periodic domains. *Dyn. Atmos. Oceans*, **7**, 67–93.
- Hodur, R. M., 1997: The Naval Research Laboratory's Coupled Ocean/Atmosphere Mesoscale Prediction System (COAMPS). *Mon. Wea. Rev.*, **125**, 1414–1430.
- Kirsch, A., 1996: *An Introduction to the Mathematical Theory of Inverse Problems*. Springer, 283 pp.
- Lehoucq, R. B., D. C. Sorensen, and C. Yang, 1998: *ARPACK Users' Guide: Solution of Large-Scale Eigenvalue Problems with Implicitly Restarted Arnoldi Methods*. Software, Environments, and Tools, Vol. 6, SIAM, 160 pp.
- Liu, D. C., and J. Nocedal, 1989: On the limited memory BFGS method for large scale optimization. *Math. Program.*, **45**, 503–528.
- Lorenc, A. C., 1986: Analysis methods for numerical weather prediction. *Quart. J. Roy. Meteor. Soc.*, **112**, 1177–1194.
- , and Coauthors, 2000: The Met Office global 3-dimensional variational data assimilation scheme. *Quart. J. Roy. Meteor. Soc.*, **126**, 2991–3012.
- Lynch, P., 1988: Deducing the wind from the vorticity and divergence. *Mon. Wea. Rev.*, **116**, 86–93.
- , 1989: Partitioning the wind in a limited domain. *Mon. Wea. Rev.*, **117**, 1492–1500.
- Marchesiello, P., J. C. McWilliams, and A. F. Shchepetkin, 2001: Open boundary conditions for long-term integration of regional ocean models. *Ocean Modell.*, **3**, 1–20.
- , —, and A. Shchepetkin, 2003: Equilibrium structure and dynamics of the California current system. *J. Phys. Oceanogr.*, **33**, 753–783.
- National Research Council, 2002: *Weather Radar Technology Beyond NEXRAD*. National Academies Press, 96 pp.
- Navon, I. M., X. Zou, J. Derber, and J. Sela, 1992: Variational data assimilation with an adiabatic version of NMC spectral model. *Mon. Wea. Rev.*, **120**, 1433–1446.
- Nocedal, J., and S. J. Wright, 1999: *Numerical Optimization*. Springer-Verlag, 656 pp.
- Palmer, C. E., 1952: Tropical meteorology. *Quart. J. Roy. Meteor. Soc.*, **78**, 126–164.
- Puduan, J. D., and H. C. Graber, 1997: Introduction to high-frequency radar: Reality and myth. *Oceanography*, **10**, 36–39.
- Sangster, W. E., 1960: A method of representing the horizontal pressure force without reduction of pressures to sea level. *J. Meteor.*, **17**, 166–176.
- Shchepetkin, A. F., and J. C. McWilliams, 1998: Quasi-monotone advection schemes based on explicit locally adaptive dissipation. *Mon. Wea. Rev.*, **126**, 1541–1580.
- , and —, 2003: A method for computing horizontal pressure-gradient force in an ocean model with a non-aligned vertical coordinate. *J. Geophys. Res.*, **108**, 3090, doi:10.1029/2001JC001047.
- Shukla, J., and K. R. Saha, 1974: Computation of non-divergent streamfunction and irrotational velocity potential from the observed winds. *Mon. Wea. Rev.*, **102**, 419–425.
- Tikhonov, A. N., and V. Arsenin, 1977: *Solution of Ill-Posed Problems*. Winston and Sons, 224 pp.
- Watterson, I. G., 2001: Decomposition of global ocean currents using a simple iterative method. *J. Atmos. Oceanic Technol.*, **18**, 691–703.